Geol. Mag. **155** (*1*), *2018, pp. 193–202.* © *Cambridge University Press 2017*
doi:10.1017/S0016756817000711

RAPID COMMUNICATION

An approach towards the projectile trajectory during the oblique Steinheim meteorite impact by the interpretation of structural crater features and the distribution of shatter cones

E. BUCHNER*

HNU - Neu-Ulm University of Applied Sciences, Wileystraße 1, D-89231 Neu-Ulm, Germany and Institut für Mineralogie und Kristallchemie, Universität Stuttgart, Azenbergstraße 18, D-70174 Stuttgart, Germany

(*Received* 5 April 2017; *accepted* 30 July 2017; *first published online* 7 September 2017)

Abstract

The distinct alignment of the Steinheim Basin and the Nördlinger Ries impact structures in SW Germany and the Central European tektite strewn field suggest ENE-directed trajectories of the Ries and Steinheim impacting bodies. From impact experiments, the asymmetry of the Steinheim crater and the arrangement of structural features therein are in good agreement with features produced during an oblique impact at 30° from the horizontal. The restriction of shatter cones to the eastern segment of the Steinheim Basin crater also suggests a west–east-directed trend of the impact direction, and supports previous models that favoured such impactor trajectory.

Keywords: Steinheim Basin, shatter cones, oblique impact, impact trajectory

1. Introduction

The *c.* 3.8 km diameter Steinheim Basin, centred at 48° 41′ N, 10° 04′ E, *c.* 42 km SW of the centre of the Ries crater, is a complex impact crater with a prominent central uplift set in a sequence of Triassic and Jurassic sedimentary rocks in SW Germany (e.g. Reiff, 1976, 1977; Heizmann & Reiff, 2002; Ivanov & Stöffler, 2005; Buchner & Schmieder, 2010, 2015; Buchner & Schmieder, 2017; Figs 1, 2). Due to the Upper Miocene post-impact sedimentary cover, removed during Quaternary times, the primary crater morphology of the Steinheim Basin is today well represented, making Steinheim one of the best-preserved complex impact craters on Earth (e.g. Heizmann & Reiff, 2002). The morphological crater rim exhibits inclined and brecciated blocks and clods of Upper Jurassic (Kimmeridgian–Tithonian) marine limestones (Heizmann & Reiff, 2002; Reiff, 2004).

A lithic impact breccia is known from numerous drillings into the Steinheim Basin (e.g. Reiff, 2004) that contains variable amounts of lithic clasts of Middle–Upper Jurassic limestones, marls, mudstones and sandstones. Although there is still no striking evidence for higher levels of shock in mineral grains, the Steinheim Basin is well known for its shatter cones (Fig. 3a) of exemplary shape and quality (e.g. Branco & Fraas, 1905; Dietz, 1959, 1960; Dietz & Butler, 1964; von Engelhardt *et al*. 1967; Heizmann & Reiff, 2002; Fig. 4). Silicate melt lithologies (Buchner & Schmieder, 2010) and carbonatic impact melt rock (Anders *et al*. 2013) were reported from the overall carbonate-dominated impact breccia of the Steinheim Basin. Although isotopic dating has not yet yielded a geologically reasonable age, the Steinheim impact structure is thought to have formed simultaneously with the *c.* 24 km Nördlinger Ries crater (e.g. Stöffler, Artemieva & Pierazzo, 2002) by the impact of a binary asteroid at *c.* 14.8 Ma (e.g. Buchner *et al*. 2013), which is roughly consistent with the Miocene post-impact crater lake biostratigraphy at both impact craters (Reiff, 1988; 2004; Buchner *et al*. 2010, Buchner & Schmieder 2013*a*, *b*; cf. Schmieder *et al*. 2014 for discussion). Fe-Ni-Co sulphides and Fe-Ni droplets associated with the Steinheim melt lithologies (Schmieder & Buchner, 2009, 2010*a*, *b*; Buchner & Schmieder, 2010; Anders *et al*. 2013) and possibly hydrothermally altered minerals on shatter cone surfaces suggest a general affinity towards an iron meteoritic source (Buchner & Schmieder, 2010, 2013*a*).

Deformation caused by the Steinheim impact mainly affected Jurassic sedimentary rocks. Crater-filling impact breccias contain abundant clasts of Upper–Middle Jurassic rocks, whereas fracturing, faulting and structural uplift (*c.* 350 m at the centre of the Steinheim Basin) reaches down to the Upper Triassic Keuper sandstones (e.g. Heizmann & Reiff, 2002; Reiff, 2004; Buchner & Schmieder, 2013*b*, their fig. 5). Middle Jurassic (Upper Aalenian) iron-rich and locally shatter-coned marine ‘Eisensandstein’ sandstones (e.g. Schmieder & Buchner, 2013, their fig. 5; Fig. 3b) build up the flanks of the central uplift. At the centre of the Steinheim central uplift (Fig. 2), the Middle Jurassic (Lower Aalenian) marine, black shale-type ‘Opalinuston’ claystone formation crops out. Small shatter cones in nodules in this claystones (Fig. 3c) were recently described by Schmieder & Buchner (2013). The strongly squeezed Opalinus Claystone strata are, where probed, in an almost upright position in the upper parts of the central uplift and still show a *c.* 60° basin-ward inclination at a depth of 200 m (Reiff, 1976; Heizmann & Reiff, 2002).

The trajectory and the obliquity of the impactor that formed the Steinheim Basin have not been studied in detail. As the Steinheim impact structure is thought to have formed simultaneously with the Nördlinger Ries (e.g. Stöffler, Artemieva & Pierazzo, 2002; Ivanov & Stöffler,

*Author for correspondence: elmar.buchner@hs-neu-ulm.de

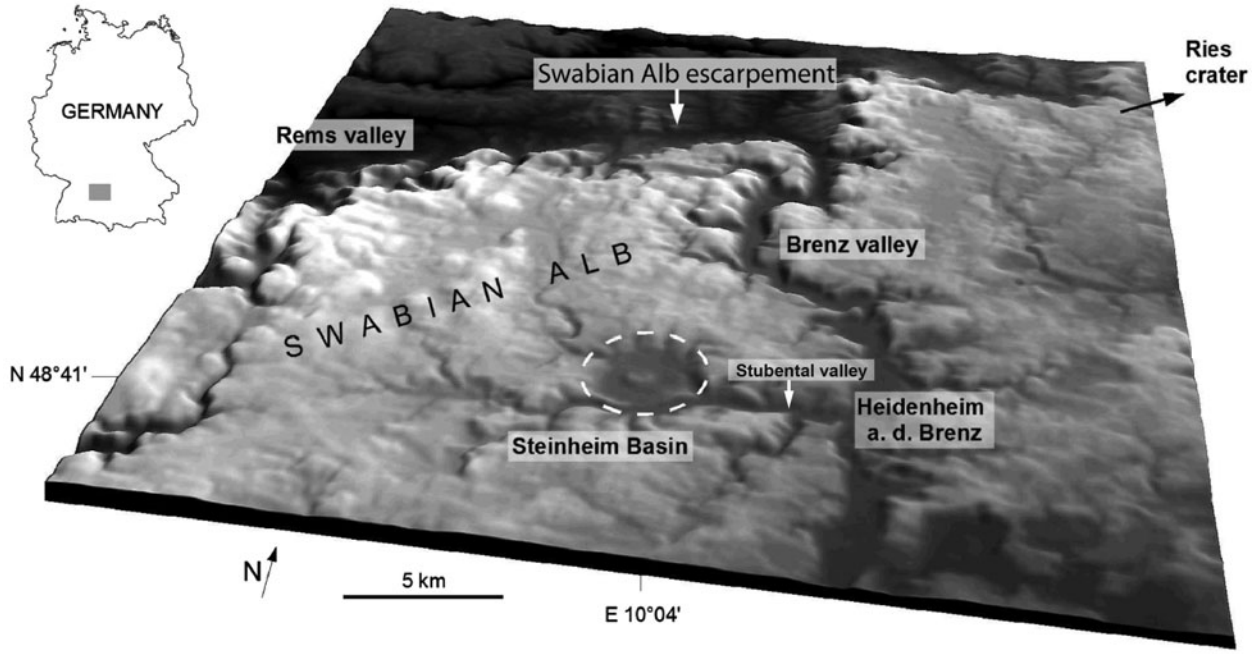

Figure 1. Shaded relief image of the eastern Swabian Alb plateau showing the position of the Steinheim Basin (dashed line indicates *c.* 3.8 km crater diameter), the adjacent valleys, main morphological features (Alb escarpment) and the position of the city of Heidenheim an der Brenz (see small map for position of the scene in SW Germany; Shuttle Radar Topography Mission data, twofold vertical exaggeration).

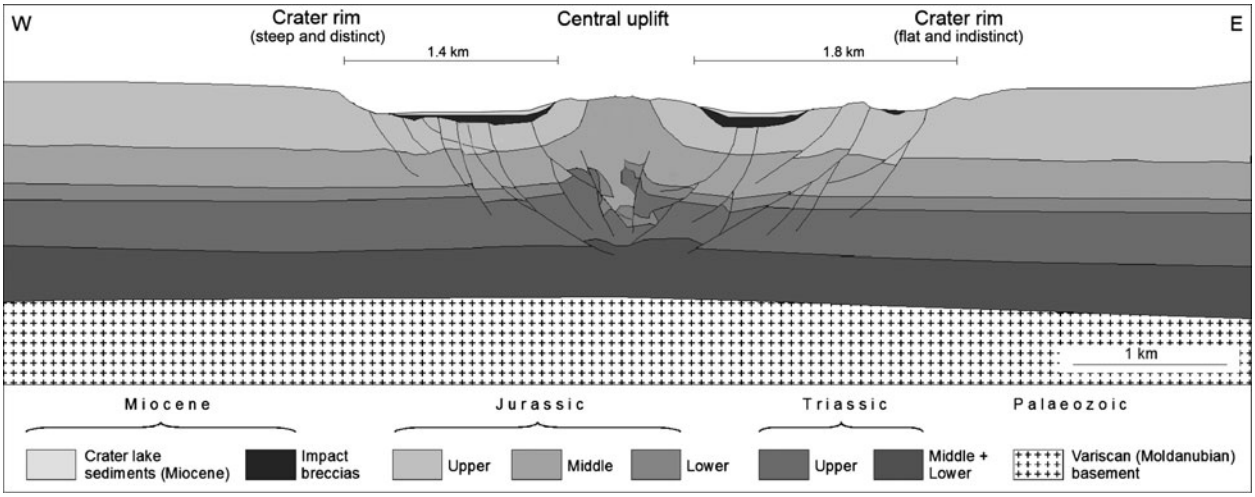

Figure 2. Schematic cross-section of the Steinheim Basin displaying the main sedimentary units of the Steinheim target rocks. The cross-section shows the asymmetry of the impact structure with a steep and distinct western crater rim and the somewhat elongated eastern part of the crater with a more flat and indistinctly developed crater rim (modified from Schmieder & Buchner 2013; after Mattmüller, 1994 and Reiff, 2004). Vertical exaggeration *c.* ×1.5.

2005), an identical or at least similar impactor trajectory of both parts of the binary asteroid would be expected. The alignment of the Steinheim Basin, the Ries crater and the Central European tektite strewn field requires an oblique impact of a binary asteroid from a WSW direction to explain the position of the craters and the distribution of the individual moldavite sub-strewn fields (e.g. Stöffler, Artemieva & Pierazzo, 2002). Based on numerical modelling, an impact at 30° (from the horizontal) and at an impact velocity of 20 km s^{-1} is in good agreement with the formation of the Ries crater and the moldavite strewn field. Similar parameters are also presumed for the Steinheim Basin impact event (Stöffler, Artemieva & Pierazzo, 2002).

2. The occurrence and distribution of shatter cones in the Steinheim Basin

Among a number of structural features suggestive of meteorite impact on Earth, shatter cones are the only hand-specimen-scale features currently accepted as convincing evidence for shock metamorphism (e.g. French & Short, 1968; French, 1998; Langenhorst, 2002; French & Koeberl,

https://doi.org/10.1017/S0016756817000711 Published online by Cambridge University Press

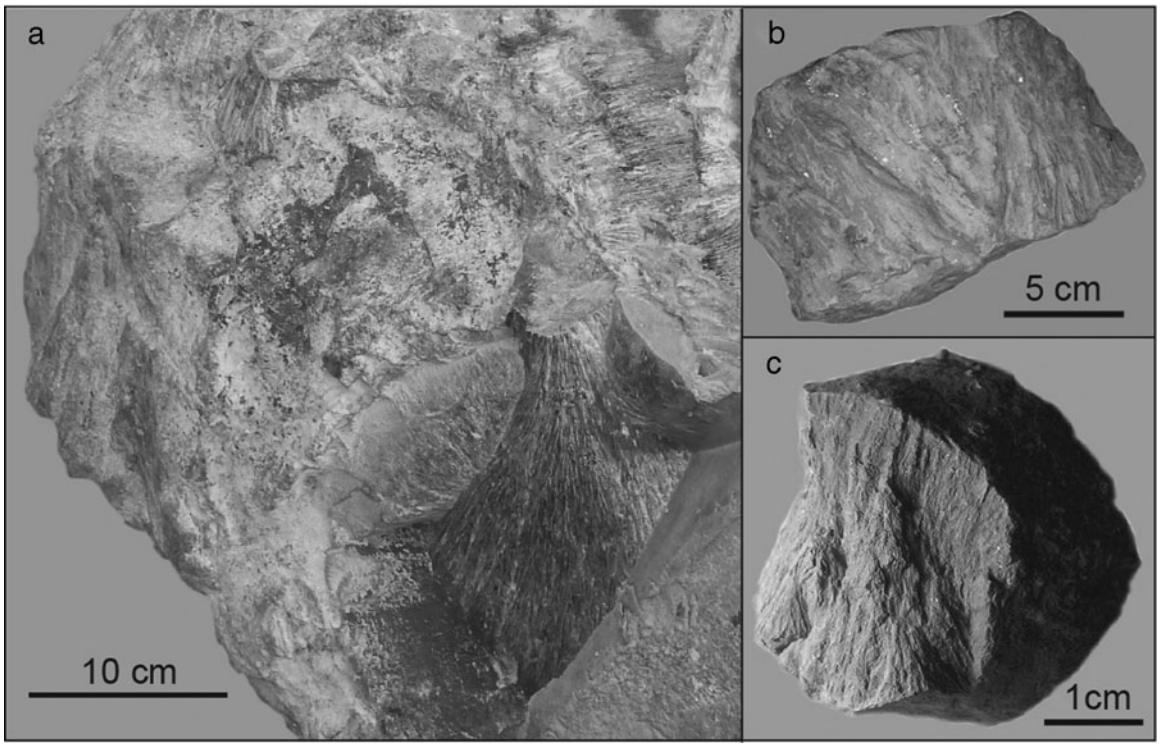

Figure 3. (a) Shatter cones in a block of Upper Jurassic limestones (Kimmeridgian–Tithonian) found at the eastern morphological crater rim. (b) Fairly well-developed shatter cones in Middle Jurassic sandstone (Eisensandstein Formation; Aalenian) from the south-eastern flank of the central uplift. (c) Shattered concretion from Middle Jurassic claystones (Opalinuston Formation, Aalenian) from the top of the central uplift of the Steinheim Basin (see Table 1 for more details).

2010). According to Nicolaysen & Reimold (1999), shatter cones are represented by a range of curved to curvilinear fractures decorated with more or less divergent striations. Striations radiate from an apex of a conical feature or from a narrow (a few millimetres to a few centimetres wide) apical area. The striation geometry is distinctive: ridges and valleys generally have smooth surfaces and are well rounded. Shatter cones are thought to form in response to rapid and dynamic tensile stresses during impact (Sagy, Reches & Fineberg, 2002; Sagy, Fineberg & Reches, 2004; Osinski & Ferrière, 2016) by the interference of shock waves at shock pressures of *c.* 2 GPa onwards (Baratoux & Melosh, 2003). On the basis of field mapping in several impact structures, Osinski & Ferrière (2016) determined that the formation of *in situ* shatter cones is restricted to the target rocks in the centre (up to 0.4 × the radius) of the crater. An extended discussion of the properties and the origin of shatter cones is given in Baratoux & Reimold (2016).

In the Steinheim Basin, well-developed shatter cones are known from Upper Jurassic limestones (e.g. Heizmann & Reiff, 2002) and from Middle Jurassic iron-rich and locally shatter-coned marine 'Eisensandstein' sandstones. Moreover, morphologically variable shatter cones were described from concretions of the Middle Jurassic Opalinus Claystone by Schmieder & Buchner (2013). Allochthonous limestone shatter cones also occur in the basin breccia (e.g. Heizmann & Reiff, 2002). Small limestone shatter cones were encountered in the drill cores numbers 19 and 32 (Reiff, 2004) from drillings that penetrated the basin breccia in the eastern crater sector (Table 1). Autochthonous limestone shatter cones are commonplace in Upper Jurassic rocks forming the structural crater floor, mainly in the eastern and southeastern parts of the crater (Figs 4, 5). These types of shatter cone (locally from Middle Jurassic iron sandstones) are also known from rocks that build up the northeastern and eastern flanks of the central uplift. In the central domain of the central uplift, the Middle Jurassic Opalinus Claystone is known to contain shatter cones in concretionary clay- and marlstone nodules (Schmieder & Buchner, 2013). However, shatter cone occurrence is not restricted to the central parts of the structure; it also extends to the eastern morphological crater rim. All locations where shatter cones were found in the Steinheim Basin are illustrated in Figures 4 and 5 and listed in Table 1.

3. Structural features of the Steinheim Basin crater: methods and results

A compiled tectonic map of the Steinheim Basin (Fig. 5) was generated from the geological map (GK Heidenheim 1:25 000; Reiff, 2004) and from the historic geological map of the Steinheim Basin (Geologische Spezialkarte des Steinheimer Beckens; Kranz, 1923), as well as from the very detailed lineament pattern map of the study area (Reiff, 2004). Additionally, Landsat imagery (GeoBasis-DE/BKG 2009, Heidenheim an der Brenz, map data provided by Bundesamt für Kartographie und Geodäsie, Frankfurt am Main) were analysed. Known and field-proven faults were taken from the geological maps mentioned. The lineament map for the Steinheim area was analysed and all lineaments that do not correspond to the known lineament pattern of southern Germany were integrated in the map (Fig. 5a; compare to Fig. 5c). Likely faults were plotted by analysis of the morphological features and lineament pattern of the Steinheim Basin apparent in Landsat imagery. Assuming that the drainage system around the impact crater preferentially developed along tectonic features, further faults

https://doi.org/10.1017/S0016756817000711 Published online by Cambridge University Press

Table 1. Compilation of the locations and dates of shatter cone findings in the Steinheim Basin and their relation to the structural features of the impact crater as available from literature, personal sampling and information from local shatter cone collectors.

Locality	Type of rock	Description	Geological setting	Date of finding	Reference
Borehole (no. 19); southern basin (48° 40′ 49″ N, 10° 03′ 50″ E)	Impact breccia	Small shatter cone in marly limestone in basin breccia	Allochthonous shatter cone in impact ejecta; inside the crater	1964	Reiff (2004)
Borehole (no. 32), southeastern basin (48° 40′ 32″ N, 10° 04″ 20″ E)	Impact breccia	Small shatter cone in marly limestone in basin breccia	Allochthonous shatter cone in impact ejecta; inside the crater	1965	Reiff (2004)
Temporary outcrop (excavation pit) at the eastern morphological crater rim; Figure 3a (48° 41′ 10″ N, 10° 05′ 23″ E)	Upper Jurassic limestones (Kimmeridgian–Tithonian)	Small and large (decimetre-sized), well-developed shatter cones; large blocks with excellent shatter cone individuals in various directions	Shatter cones in parautochthonous blocks forming the morphological crater rim	1997	Pers. comm. E. Stabenow, 2017 (Steinheim am Albuch); big block stored at the Meteorkrater-Museum Steinheim
Fields and excavation pits along the eastern crater rim (west of Galgenbergweg) (48° 41′ 26″ N, 10° 04′ 32″ E)	Upper Jurassic limestones (Kimmeridgian–Tithonian)	Large limestone blocks with excellently developed, decimetre-sized shatter cone individuals in various directions	Shatter cones in rocks forming the structural crater floor	2002	Schmieder & Buchner (2013), their figure 3
Temporary outcrops (excavation pits) on the northern flank of the central uplift	Upper Jurassic limestones (Kimmeridgian–Tithonian)	Limestone blocks with excellently developed, large (decimetre-sized) shatter cone individuals in various directions	Central uplift	Prior to 2002; until today in temporary outcrops	Heizmann & Reiff (2002), their figure 68; stored at the Meteorkrater-Museum Steinheim
Fields along the SE crater rim (northern flanks of Burgstall and Knill) (48° 40′ 42″ N, 10° 04′ 36″ E)	Upper Jurassic limestones (Kimmeridgian–Tithonian)	Large limestone shatter cone individuals (centimetre- to decimetre-sized)	Shatter cones in rocks forming the structural crater floor	2002–2013, shatter cones are found frequently at this site)	Schmieder & Buchner (2013), their figure 3
Temporary outcrop along the newly constructed country road L1163 (Galgenberg-Scholle), eastern crater rim (48° 41′ 09″ N, 10° 05′ 04″ E)	Upper Jurassic limestones (Tithonian)	Large limestone blocks with excellently developed, large (decimetre-sized) shatter cone individuals in various directions	Shatter cones in parautochthonous blocks forming the morphological crater rim	2003–2004	Schmieder & Buchner (2013), their figure 3
Temporary outcrop (excavation pit of a newly constructed private building) at the northern flank of the central uplift; Figure 3b (48° 41′ 17″ N, 10° 04′ 07″ E)	Middle Jurassic sandstone (Eisensandstein Formation; Aalenian)	Fairly well-developed single (centimetre-sized) sandstone shatter cones	Central uplift	2009	Schmieder & Buchner (2013), their figure 4; stored at ZERIN, Nördlingen
Temporary outcrop (excavation pit of a newly constructed kindergarten) at the top of the central uplift (48° 41′ 17″ N, 10° 04′ 07″ E)	Upper Jurassic limestones (Kimmeridgian–Tithonian)	Large limestone block (40×18×19 cm) with excellently developed, large (decimetre-sized) shatter cone individuals in various directions	Central uplift	October 2010	Pers.comm. P. Seidel, 2017 (Steinheim am Albuch)
Temporary excavation pit (water catchment) on top of the central uplift; Figure 3c	Middle Jurassic claystones (Opalinuston Formation, Aalenian)	Shattered concretions showing small (millimetre- to centimetre-sized) excellently developed shatter cone individuals in various directions	Central uplift	2010	Schmieder & Buchner (2013)

https://doi.org/10.1017/S0016756817000711 Published online by Cambridge University Press

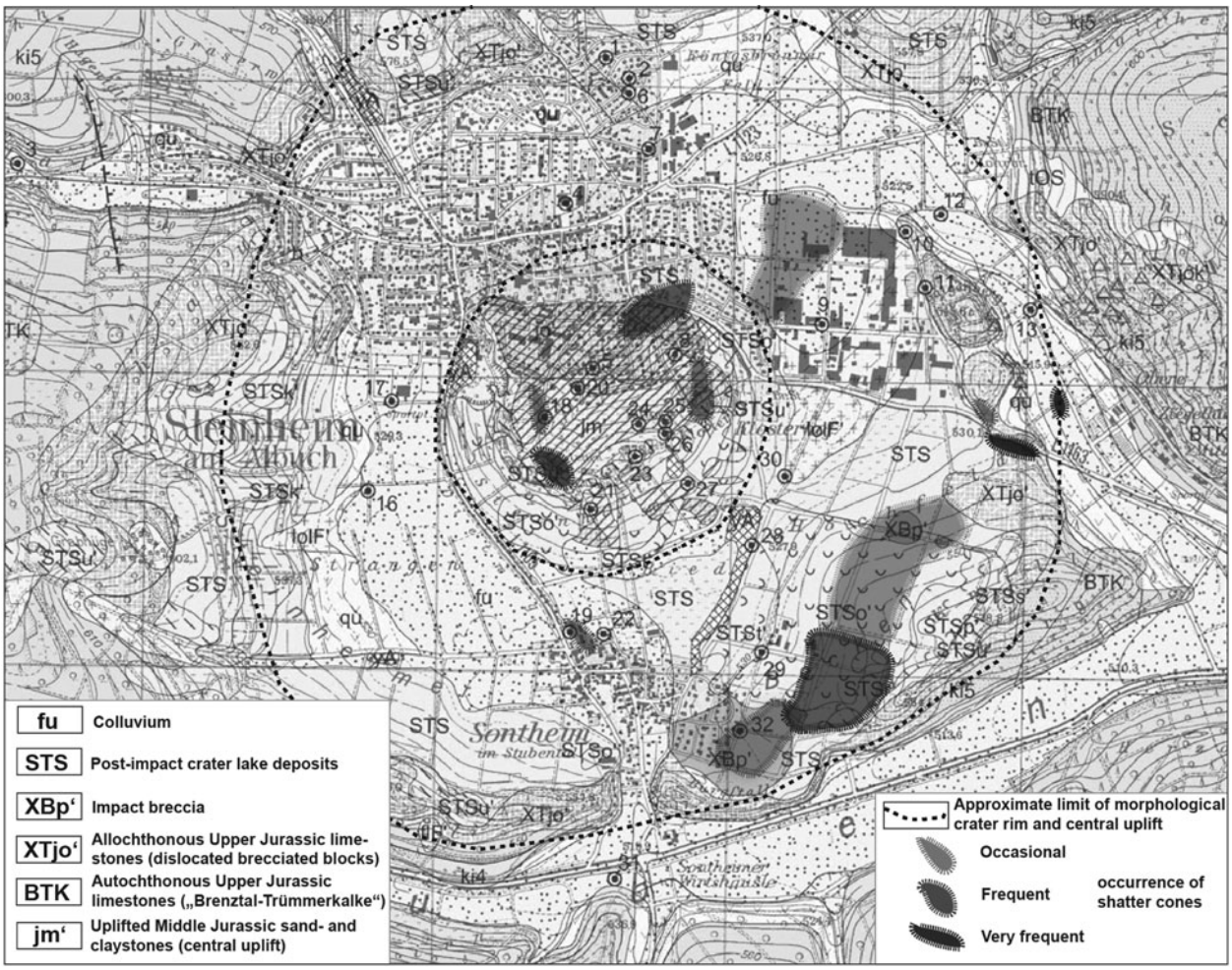

Figure 4. Section of the geological map (GK Heidenheim 1:25 000; Reiff, 2004) showing the Steinheim Basin impact crater with the main geological units exposed and the occurrence of shatter cones in the central and eastern part of the structure, compiled from the literature and from field experience and sampling activities over the past three decades. The locations where shatter cones are found do not seem to be directly linked to any of the geological units but are linked to localities where the structural crater floor is exposed or only slightly covered by thin colluvium or upper Miocene crater lake deposits. Basically, the geological situation in the southern, western and northern portion of the crater is similar but the locations of shatter cones are restricted to the eastern crater section.

(failure pattern in the sense of Schultz & Anderson, 1996) in the periphery of the crater were plotted along existing dry valleys.

The analysis of the resulting fault pattern and the schematic cross-section of the Steinheim Basin highlights how the impact structure seems to be morphologically elongated along a west–east-directed axis (Fig. 2), and the excavation depth of the crater (e.g. Reiff, 1976, 2004) seems to decrease eastwards. This results in a horizontal and vertical asymmetry of the entire structure: a steep and pronounced western, and a shallow and unpronounced eastern crater rim (compare to Figs 2, 5). The morphological asymmetry of the central uplift is clearly apparent by a very steep western and a rather gentle eastern flank of the central peak (Fig. 5). The topographically highest point of the central uplift lies at an elevation of *c.* 574 m, off-centre towards the western flank. In the eastwards extension of the central peak, a radially orientated, morphological depression is obvious that today appears as the dry valley of the 'Stubental'. The centre of symmetry of the crater is offset eastwards, and is therefore not identical to the centre of the central peak. The outer failure zone forms an incomplete, subarcuate fracture pattern in which faults are centred in the east, resulting in apparently less surface failure in the western periphery compared to the eastern part of the crater.

4. Discussion

4.a. Distribution of the shatter cones

The occurrence of Steinheim shatter cones is concentrated in the eastern (and southeastern) crater sector (Figs 4, 5). This observation raises the following questions that may explain this restriction.

(1) Might poor outcrop conditions in the other crater sectors be responsible for the preferential finding of shatter cones in the eastern and southeastern crater sector? Findings of shatter cones are often linked to localities where the structural crater floor is exposed or only covered by thin colluvium, crater lake deposits and/or soil. Parautochthonous inclined and brecciated blocks and clods of Upper Jurassic (Kimmeridgian–Tithonian) marine limestones (unit XTjo′ in Fig. 4), which form the outer part of the structural crater floor and the morphological crater rim, are more or less uniformly exposed around the entire crater (e.g. at the 'Galgenberg' clod). Nevertheless, the occurrence of shatter cones in

https://doi.org/10.1017/S0016756817000711 Published online by Cambridge University Press

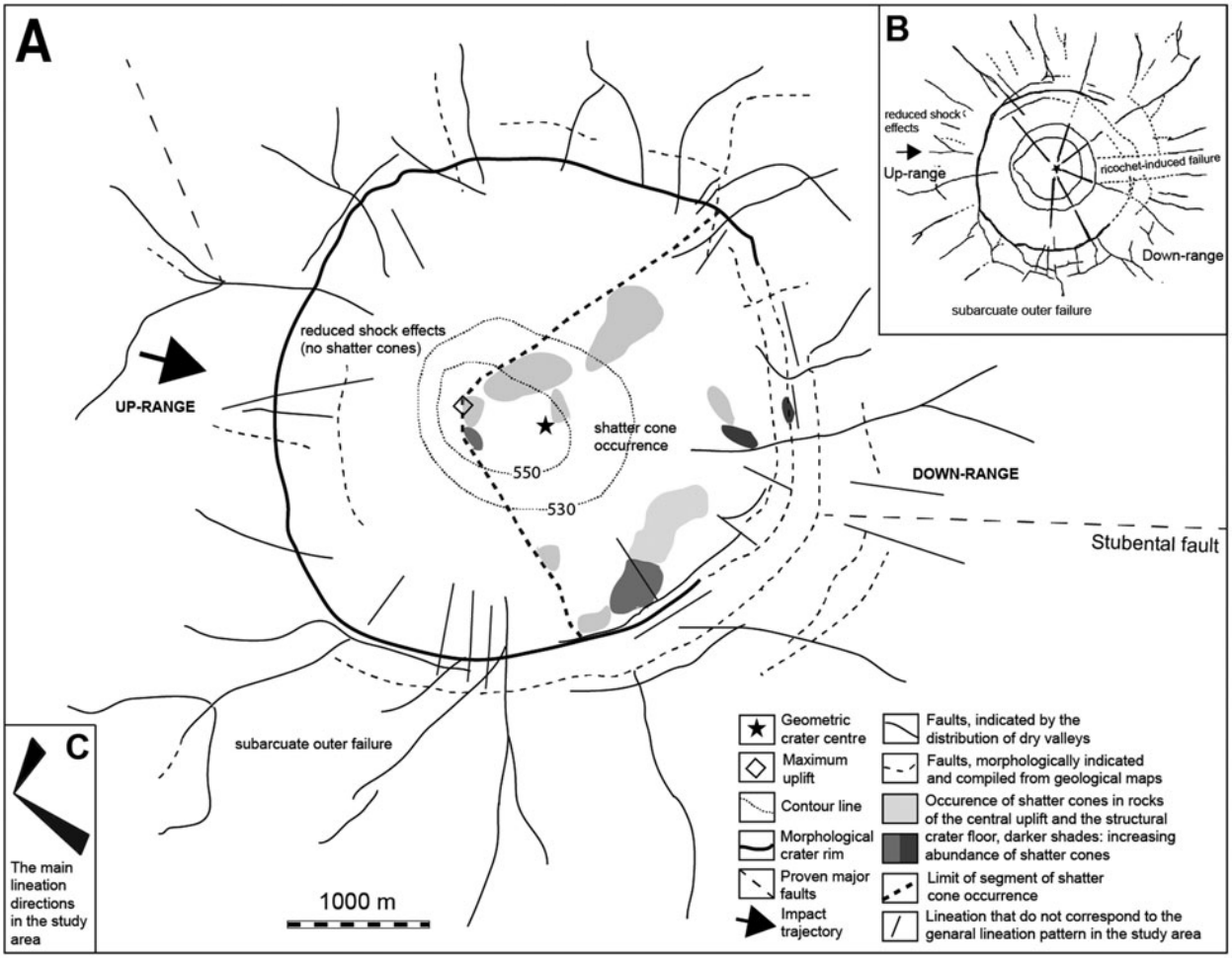

Figure 5. Map of tectonic patterns of (a) the Steinheim Basin and (b) an impact structure experimentally created by an oblique impact at 15° from the horizontal into dry ice by Schultz (1994) and Schultz & Anderson (1996). Faults and lineations for the Steinheim Basin are compiled from the geological map (GK Heidenheim 1:25 000; Reiff, 2004) and from the lineation map 1:25 000; Reiff, 2004), from the geological map of the Steinheim Basin (Geologische Spezialkarte des Steinheimer Beckens; Kranz, 1923) and from Landsat imagery (GeoBasis-DE/BKG 2009). Both structures display striking similarities with respect to the crater asymmetry, the shifting of the centre of symmetry and the arrangement of the proposed fault patterns. The absence of shatter cones in the crater sector with reduced shock effects (up-range) and the occurrence of shatter cones in the down-range direction of the crater also suggest an impactor trajectory that generally trends west–east. (c) Rose diagram illustrating the main regional lineation directions in the study area. Note that the (probably impact-induced) lineation patterns in and around the Steinheim Basin do not correspond to these main lineation directions.

these displaced blocks is restricted to the eastern crater sector. As a result, outcrop conditions do not favour the finding of shatter cones in any part of the structure.

(2) Might shatter cones have formed preferentially in specific types of rocks? The inclined and brecciated blocks and clods of Upper Jurassic limestones around the crater do not exhibit any essential variations of facies (e.g. Reiff, 2004). Furthermore, shatter cones also occur in bedded as well as in massive limestones in the eastern crater sector. Shatter cones occur in breccia-hosted lithic clasts known from drill cores in the eastern and southeastern part of the crater (e.g. borehole numbers 19, drilled in 1964, and 32, drilled in 1965) (Reiff, 2004; see Table 1), but were not described from impact breccia probed at other crater sectors (e.g. from borehole numbers 16 (1965) and 17 (1979) drilled in the western crater sector, and borehole numbers 1 and 2 (1965) and 7 (1969) and 4 (1972/1973), drilled in impact breccias of the northern crater basin; Reiff, 2004). Clasts derived from the basin breccia can be sampled at the surface over the entire crater, but the finding of shatter cones in these components is again restricted to the eastern (and southeastern) crater section. The most promising places for finding shatter cones do not seem to be linked directly to any specific geological unit across the Steinheim Basin.

(3) Did the heterogeneous propagation of the peak shock pressure, caused by the presumed obliquity of the incoming projectile, result in higher pressures in the target rocks of the eastern crater sector, that is, in the down-range direction? The level of shock-metamorphic effects in the target rocks of the Steinheim Basin is generally rather low (indicating up to *c.* 2–5 GPa) and was only capable of producing shatter cones. Although von Engelhardt *et al.* (1967) reported shocked quartz grains from sandstones of the deeper parts of the target rocks, there is still no striking evidence for higher levels of shock in mineral grains in the Steinheim Basin (see also Buchner & Schmieder, 2010). The relatively low level of shock-metamorphic overprint might be explained by a buffering effect induced by the compaction of the highly porous target rocks and the waste of kinetic energy by the collapse of free pore space, such as large-scale karst cavities and the effective porosity of the sedimentary target rocks on a mineral scale (Buchner & Schmieder, 2015). According

https://doi.org/10.1017/S0016756817000711 Published online by Cambridge University Press

to Poelchau et al. (2015), a further process, namely $CaCO_3$ dissociation or devolatization, could have impeded the shock wave, although devolatization to $CaO + CO_2$ occurs at relatively high shock pressures. By the use of hydrocode impact modelling, Pierazzo & Melosh (2000) have shown that the peak shock pressure generally decreases with increasing obliquity of impact processes. The impact angle additionally affects the distribution and magnitude of shock waves generated by an impact (Dahl & Schultz, 1999). The peak pressure in a propagating shock wave usually follows a power-law decay curve, but the magnitude in the down-range direction can be significantly higher in comparison to the up-range direction (e.g. Pierazzo & Melosh, 2000). According to impact experiments by Ai & Ahrens (2005), shock-induced damage beneath oblique craters in the down-range direction is stronger than in the up-range direction. Strain-rate measurements in oblique impact experiments have shown that their magnitude is about twice in the target down-range direction at the same peak stress (Dahl & Schultz, 1999). Taking all these factors into account, the apparent restriction of shatter cones to the eastern (and southeastern) crater sector might be explained most plausibly by an oblique Steinheim Basin impact with an impactor trajectory of WNW–ESE (compare to Figs 4, 5), where shock pressures were sufficient to produce shatter cones down-range in the eastern crater sector but too low to generate shatter cones in the up-range (western) direction.

4.b. Structural features of the Steinheim Basin crater

Impact craters produced by oblique impacts are often elongated along the impactor trajectory, and may also show a distinct 'bilateral' asymmetry of their central uplifts (e.g. Howard, Offield & Wilshire, 1972; Milton *et al*. 1972; Scherler, Kenkmann & Jahn, 2006; Kenkmann *et al*. 2010). Asymmetry increases dramatically in solid targets at lower angles, as the elliptical projectile 'footprint' extends excavation down-range from the point of impact (e.g. Dahl & Schultz, 2001). In analogy, the apparent tectonic failure pattern and the schematic cross-section of the Steinheim Basin reveal an elongated crater structure along a west–east-directed axis (Fig. 2), with a steep western crater rim (up-range) and decreasing excavation depth eastwards, resulting in a shallow and unpronounced eastern crater rim (down-range; compare to Figs 2, 5). For the elliptic Matt Wilson impact structure in Australia, Kenkmann & Poelchau (2009) also reported a highly oblique impact accompanied by a steepened up-range crater rim. This is consistent with the observations by Schultz & Anderson (1996) that oblique impacts result in the greatest penetration up-range with shallower penetration down-range. The up-range wall slope of impact craters on the Moon, Mars and Mercury is also typically steeper than the down-range wall slope (Herrick, 2017). In oblique impact experiments, Schultz & Anderson (1996) showed that central peaks in complex craters are offset up-range, and that the centre of symmetry of the resultant impact crater is offset down-range from the point of deepest penetration (Schultz, 1994; Fig. 5b). In complex impact craters with central peaks, the point of deepest penetration is probably represented by the morphologically highest point of the central uplift, corresponding to the highest net amount of structural uplift during the excavation to modification state (Dahl & Schultz, 2001). In contrast, no obvious trends of interior asymmetries of the central peaks (central peak offset) were found for low-angle impact craters on planets such as Mars (e.g. Herrick & Hessen, 2006). Nevertheless, Figure 5a shows a pronounced up-range (i.e. westwards) offset of the central peak complex of the Steinheim Basin, and the asymmetric nature of the central peak is obvious by the very steep western (up-range, Fig. 5a) and a significantly less steep eastern flank of the central peak down-range. According to Kenkmann & Poelchau (2009), the central peak of the Matt Wilson impact structure is elongated along the symmetry axis of the elliptical structure.

The centre of symmetry of the Steinheim Basin is also offset down-range (Fig. 5a). In the eastwards extension of the central peak of the Steinheim Basin, a radially orientated, morphological depression is obvious (see Fig. 5a) that appears as the dry valley of the Stubental. The outer failure zone of an oblique impact (30° from the horizontal; Schultz, 1994) forms an incomplete, subarcuate fracture up-range but is centred down-range. The outer failure zone of the Steinheim Basin also forms an incomplete, subarcuate fracture pattern, and the faults are centred down-range resulting in less surface failure up-range in the western periphery when compared to the down-range direction. As a result, the fault patterns of the Steinheim Basin surprisingly match those obtained for a 30° oblique impact in the experiments of Schultz (1994), yet at a much larger scale. The structural features of the Steinheim Basin and the experimentally obtained crater also display striking similarities with respect to the crater asymmetry and the offset of the centre of symmetry down-range. The absence of shatter cones in the crater sector with reduced shock effects (up-range; Schultz, 1994) and the occurrence of shatter cones in the down-range direction of the crater also suggest an impactor trajectory that generally trends west–east.

4.c. Obliquity and trajectory of the Ries/Steinheim impactors

An oblique impact of a binary asteroid in an ENE direction is supported by the alignment of the Steinheim Basin, the Ries crater and the Central European tektite strewn field, and can plausibly explain the locations of the two craters and the formation and distribution of moldavites (Stöffler, Artemieva & Pierazzo, 2002). The occurrence of the Steinheim shatter cones restricted to the eastern sector, as well as the structural features of the crater described in Sections 2 and 3 (Figs 2–5), also suggest a generally west–east direction of the Steinheim impactor, maybe with a slight southwards tendency at *c.* 100° bearing. The conclusions of this study lend additional support to the previous presumption that the impactor trajectory for the Ries–Steinheim impact was approximately WSW to ENE (Stöffler, Artemieva & Pierazzo, 2002). The slight discrepancy of 20–30° between the impactor trajectory from this study compared to the model results of Stöffler, Artemieva & Pierazzo (2002) might be explained by slightly differing relative movement of the two extraterrestrial bodies that formed the Ries and Steinheim impact craters. Although the larger Ries impactor may have moved in an ENE direction, the smaller Steinheim impactor that orbited the bigger of the two incoming asteroids could have hit the ground at a slightly divergent direction. Further deviation may be due to uncertainties in the analysis of tectonic features associated with the Steinheim impact event, and/or in modelling of the Ries–Steinheim impact scenario.

According to Stöffler, Artemieva & Pierazzo (2002), the binary asteroid responsible for the formation of the two impact structures in southern Germany consisted of two bodies, probably *c.* 1.5 and 0.15 km in diameter and with a pre-impact asteroid-to-asteroid spacing distance of some tens of kilometres. They impacted the target area at an angle of *c.* 30–50° from the horizontal (land surface), in a WSW–ENE direction. Simulation results for a Ries-sized impact by Stöffler, Artemieva & Pierazzo (2002) combined with the

https://doi.org/10.1017/S0016756817000711 Published online by Cambridge University Press

results obtained by Artemieva (2002) excluded an impact angle below 30° (from the horizontal) for the Ries; for an impact angle of < 30° the target-derived impact melt would contain significant contamination from the projectile, which is not the case (e.g. Schmidt & Pernicka, 1994). An impact angle of *c.* 30° is the most favourable for the tektite-type impact melt and vapour-condensate production as it occurred during the Ries impact (Stöffler, Artemieva & Pierazzo, 2002, fig. 4). The tectonic fault pattern of the Steinheim Basin strikingly matches those obtained for a 30° oblique impact by experiments of Schultz (1994) and Dahl & Schultz (2001). A low-impact angle of 30° is also consistent with the generally relatively low grade of shock metamorphism (e.g. Dahl & Schultz, 2001) in the Steinheim Basin (e.g. Buchner & Schmieder, 2010, 2015), and the reduced peak shock pressure up-range as opposed to higher shock pressures down-range observable in the Steinheim Basin. The contamination of the Steinheim target rocks by meteoritic matter as postulated by Buchner & Schmieder (2017) is also consistent with a rather shallow oblique impact. We therefore favour an impact angle of *c.* 30° for the oblique Steinheim Basin impact in accordance with the impact angle for the Ries impact proposed by Stöffler, Artemieva & Pierazzo (2002).

In the Steinheim Basin, the occurrence of shatter cones is not restricted to the centre of the crater as proposed by Osinski & Ferrière (2016) for other impact structures. Shatter cones are also present in limestone rocks forming the eastern morphological crater rim (Fig. 3a) and far beyond the 0.4 × crater radius suggested by Osinski & Ferrière (2016). The structure of the crater was reconstructed by Reiff (1976, 1977, 2004) and Groschopf & Reiff (1969) on the basis of a narrow-spaced network of drillings, and the resulting cross-section does not feature any evidence that the limestone blocks forming the eastern morphological crater rim might be dislocated over a large distance in the sense of transport from the inner crater zone towards the crater rim. The model of a shatter cone restriction to the inner crater zone in a 0.4 crater radius in the sense of Osinski & Ferrière (2016) therefore cannot be adopted for the Steinheim Basin. The extent of the shatter cones to the eastern morphological crater rim might also be explained by the west–east-directed projectile trajectory and by the highly oblique impact.

5. Conclusions

Shatter cones in the Steinheim Basin are restricted to an eastern (and southeastern) segment of the impact crater. The tectonic pattern and related structural features of the Steinheim Basin strikingly match those for an impact structure obtained from the experiments of Schultz (1994) and Dahl & Schultz (2001), formed by an oblique impact with a trajectory that deviates 30° from the horizontal. An impact angle of *c.* 30° for the oblique Steinheim impact matches the impact angle postulated for the Ries impact. These results suggest a general west–east-directed trend of the Steinheim impactor trajectory and support the binary impact model of Stöffler, Artemieva & Pierazzo (2002). A discrepancy of 20–30° between the impact trajectory for the Ries impactor reported by Stöffler, Artemieva & Pierazzo (2002) and the model for the Steinheim impact do not necessarily argue against the simultaneous formation of both craters during a Miocene double impact event. This may instead be due to uncertainties in the analysis of tectonic features associated with the Steinheim impact event, and/or by a slightly differing relative movement of the two extraterrestrial bodies that formed the double crater system.

Acknowledgements. The author is grateful to Martin Schmieder, Houston, for helpful comments and suggestions on an earlier draft of the manuscript and to Peter Seidel, Steinheim am Albuch and Tamara Luckas, town hall of Steinheim am Albuch, for helpful hints on former shatter cone locations. I am also grateful for the very helpful reviews of an anonymous reviewer and of Adam A. Garde as well as for editorial handling by Peter Clift. The author acknowledges a grant (project 11050) by the Stifterverband für die Deutsche Wissenschaft (Dieter Schwarz Stiftung).

References

Ai, H. & Ahrens, T. J. 2005. Shock-induced damage beneath normal and oblique impact craters. Houston, Texas, Lunar and Planetary Institute. In *Proceedings of 36th Lunar and Planetary Science*, abstract 1243, CD-ROM.

Anders, D., Buchner, E., Schmieder, M. & Kegler, P. 2013. Varietäten von Schmelzelithologien in den Impaktiten des Steinheimer Beckens (SW-Deutschland). *Zeitschrift der Deutschen Gesellschaft für Geowissenschaften (German Journal of Geosciences)* **164**, 491–501.

Artemieva, N. A. 2002. Tektite origin in oblique impact: Numerical modeling. In *Meteorite Impacts in Precambrian Shields* (eds Y. Plado & L. Pesonen), pp. 257–76. Berlin, Germany: Springer Verlag.

Baratoux, D. & Melosh, H. J. 2003. The formation of shatter cones by shock wave interference during impacting. *Earth and Planetary Science Letters* **216**, 43–54.

Baratoux, D. & Reimold, W. U. 2016. The current state of knowledge about shatter cones. Introduction to the Special Issue on 'Shatter Cones – Nature and Genesis'. *Meteoritics and Planetary Science* **51**(8), 1389–434.

Branco, W. & Fraas, E. 1905. Das kryptovulcanische Becken von Steinheim. Abhandlungen der königlich preussischen Akademie der Wissenschaften zu Berlin. *Physikalisch Abhandlungen* **1**, 1–64 (in German).

Buchner, E. & Schmieder, M. 2010. Steinheim suevite – a first report of melt-bearing impactites from the Steinheim Basin (SW Germany). *Meteoritics and Planetary Science* **45**, 1093–107.

Buchner, E. & Schmieder, M. 2013*a*. Das Ries-Steinheim-Ereignis – Impakt in eine miozäne Seen- und Sumpflandschaft. *Zeitschrift der Deutschen Gesellschaft für Geowissenschaften (German Journal of Geosciences)* **164**, 459–70.

Buchner, E. & Schmieder, M. 2013*b*. Der Steinheimer Suevit – schmelzeführende Impaktite aus dem Steinheimer Becken, Südwestdeutschland. *Zeitschrift der Deutschen Gesellschaft für Geowissenschaften (German Journal of Geosciences)* **164**, 471–90.

Buchner, E. & Schmieder, M. 2015. The Steinheim Basin impact crater (SW-Germany) – Where are the ejecta? *Icarus* **250**, 529–43.

Buchner, E. & Schmieder, M. 2017. Rare metals on shatter cone surfaces from the Steinheim Basin (SW Germany) – remnants of the impacting body? *Geological Magazine*, published online 13 February 2017. doi: https://doi.org/10.1017/S0016756816001357.

Buchner, E., Schwarz, W. H., Schmieder, M. & Trieloff, M. 2010. Establishing a 14.6 ± 0.2 Ma age for the Nördlinger Ries impact (Germany) – a prime example for concordant isotopic ages from various dating materials. *Meteoritics and Planetary Science* **45**, 662–74.

Buchner, E., Schwarz, W. H., Schmieder, M. & Trieloff, M. 2013. Das Alter des Meteoritenkraters Nördlinger

https://doi.org/10.1017/S0016756817000711 Published online by Cambridge University Press

Ries – eine Übersicht und kurze Diskussion der neueren Datierungen des Riesimpakts. *Zeitschrift der Deutschen Gesellschaft für Geowissenschaften (German Journal of Geosciences)* **164**, 433–45.

Dahl, J. M. & Schultz, P. H. 1999. In-target stress wave momentum content in oblique impacts. Houston, Texas, Lunar and Planetary Institute. In *Proceedings of 30th Lunar and Planetary Science*, abstract 1854, CD-ROM.

Dahl, J. M. & Schultz, P. H. 2001. Measurement of stress wave asymmetries in hypervelocity projectile impact experiments. *International Journal of Impact Engineering* **26**, 145–55.

Dietz, R. S. 1959. Shatter cones in cryptoexplosion structures (meteorite impact?). *The Journal of Geology* **67**, 496–505.

Dietz, R. S. 1960. Meteorite impact suggested by shatter cones in rock. *Science* **131**, 1781–4.

Dietz, R. S. & Butler, L. W. 1964. Shatter-cone orientations at Sudbury, Canada. *Nature* **4**, 204–5.

French, B. M. 1998. Traces of catastrophe: a handbook of shock-metamorphic effects in terrestrial meteorite impact structures. LPI Contribution no. 954, Lunar and Planetary Institute, Houston TX, 120 pp.

French, B. M. & Koeberl, C. 2010. The convincing identification of terrestrial meteorite impact structures: what works, what doesn't, and why. *Earth-Science Reviews* **98**, 123–70.

French, B. M. & Short, N. M. (eds) 1968. *Shock Metamorphism of Natural Materials*. Baltimore, Maryland, USA: Mono Book, 644 pp.

Groschopf, P. & Reiff, W. 1969. Das Steinheimer Becken. Ein Vergleich mit dem Ries. *Geologica Bavarica* **61**, 400–12 (in German).

Heizmann, E. P. J. & Reiff, W. 2002. *Der Steinheimer Meteorkrater*. Munich: Pfeil, 160 pp. (in German).

Herrick, R. R. 2017. Small impacts and small impactors. In *Proceedings of 48th Lunar and Planetary Science Conference*, 20–24 March. The Woodlands, Texas, Abstract #2803.

Herrick, R. R. & Hessen, K. K. 2006. The planforms of low-angle impact craters in the northern hemisphere of Mars. *Meteoritics & Planetary Science* **41**, 1483–95.

Howard, K. A., Offield, T. W. & Wilshire, H. G. 1972. Structure of Sierra Madera, Texas, as a guide to central peaks of lunar craters. *Geological Society of America Bulletin* **83**, 2795–808.

Ivanov, B. A. & Stöffler, D. 2005. The Steinheim impact crater, Germany: Modeling of a complex crater with central uplift. In *Proceedings of 36th Lunar and Planetary Science Conference*, Houston, 14–18 March. Abstract #1443.

Kenkmann, T. & Poelchau, M. H. 2009. Low-angle collision with Earth: the elliptical impact crater Matt Wilson, Northern Territory, Australia. *Geology* **37**, 459–62.

Kenkmann, T., Reimold, W. U., Khirfan, M., Salameh, E., Khoury, H. & Konsul, K. 2010. The complex impact crater Jebel Waqf as Suwwan in Jordan: effects of target heterogeneity and impact obliquity on central uplift formation. *Geological Society of America, Special Papers* **465**, 471–87.

Kranz, W. 1923. Geognostischen Spezialkarte von Württemberg (1:25.000). Atlasblatt Heidenheim. Abschnitt: Geologische Spezialkarte des Steinheimer Beckens. Württembergisches Statistisches Landesamt Stuttgart (Klett).

Langenhorst, F. 2002. Shock metamorphism of some minerals: basic introduction and microstructural observations. *Bulletin of the Czech Geological Survey* **77**, 265–82.

Mattmüller, C. R. 1994. *Ries und Steinheimer Becken. Geologischer Führer und Einführung in die Meteoritenkunde*. Stuttgart: Ferdinand Enke Verlag, 152 pp. (in German).

Milton, D. J., Barlow, B. C., Brett, R., Brown, A. R., Glikson, A. Y., Manwaring, E. A., Moss, F. J., Sedmik, E. C. E., Van Son, J. & Young, G. A. 1972. Gosses Bluff Impact Structure, Australia. *Science* **175**, 1199–207.

Nicolaysen, L. O. & Reimold, W. U. 1999. Vredefort shatter cones revisited. *Journal of Geophysical Research* **104**, 4911–30.

Osinski, G. R. & Ferrière, L. 2016. Shatter cones: (mis)understood? *Science Advances* **2**, e1600616.

Pierazzo, E. & Melosh, H. J. 2000. Hydrocode modeling of oblique impacts: the fate of the projectile. *Meteoritics and Planetary Science* **35**, 117–30.

Poelchau, M. H., Michalski, C., Deutsch, A., Thoma, K., Schäfer, F. & Kenkmann, T. 2015. Experimental Cratering in Carrara Marble: Latest Results from the MEMIN Research Unit. In *Proceedings of 46th Lunar and Planetary Science Conference*, 16–20 March, The Woodlands, Houston Texas, USA; abstract # 2447.

Reiff, W. 1976. The Steinheim Basin – A meteorite crater. Abstract presented at the Symposium on Planetary Cratering Mechanics, 13–17 September 1976, Flagstaff, AZ. *LPI Contribution* **259**, 112–4.

Reiff, W. 1977. The Steinheim Basin – An impact structure. In *Impact and Explosion Cratering: Planetary and Terrestrial Implications* (eds D. J. Roddy, R. O. Pepin & R. Merrill). Proceedings of the Symposium on Planetary Cratering Mechanics, Flagstaff, AZ, 13–17 September 1976. New York: Pergamon Press, 309–320.

Reiff, W. 1988. Zur Gleichaltrigkeit der Einschlagskrater (Meteorkrater) Steinheimer Becken und Nördlinger Ries. *Jahresberichte und Mitteilungen des Oberrheinischen Geologischen Vereins* **70**, 383–97 (in German).

Reiff, W. 2004. Geologische Karte von Baden-Württemberg 1:25000, 7326 Heidenheim, mit Erläuterungen, Landesamt für Geologie, Rohstoffe und Bergbau Baden-Württemberg, 223 pp. (in German).

Sagy, A., Fineberg, J. & Reches, Z. 2004. Shatter cones: Branched, rapid fractures formed by shock impact. *Journal of Geophysical Research* **109**, B10209, doi: 10.1029/2004/JB003016.

Sagy, A., Reches, Z. & Fineberg, J. 2002. Dynamic fracture by large extraterrestrial impacts as the origin of shatter cones. *Nature* **418**, 310–3.

Scherler, D., Kenkmann, T. & Jahn, A. 2006. Structural record of an oblique impact. *Earth and Planetary Science Letters* **248**, 43–53.

Schmidt, G. & Pernicka, E. 1994. The determination of platinum group elements (PGE) in target rocks and fall-back material of the Nördlinger Ries impact crater, Germany. *Geochimica et Cosmochimica Acta* **58**, 5083–90.

Schmieder, M. & Buchner, E. 2009. Fe-Ni-Co sulfides from the Steinheim Basin, SW Germany: possible impactor traces (abstract #5073). *Meteoritics and Planetary Science* **44**, A185.

Schmieder, M. & Buchner, E. 2010*a*. New insights into the Steinheim central uplift - part III: Shatter cones and the 'cone-in-cone' problem reloaded. In *Proceedings of the 73rd Conference of the Meteoritical Society*, 26–30 July 2010, New York, USA, abstract no. 5012.

https://doi.org/10.1017/S0016756817000711 Published online by Cambridge University Press

Schmieder, M. & Buchner, E. 2010*b*. Possible iron meteoritic contamination in impact melt particles from the Steinheim Basin (Baden-Württemberg, Germany). In *Proceedings of the 41st Lunar and Planetary Science Conference*, 1–5 March 2010, The Woodlands, Texas, USA, abstract no. 2103.

Schmieder, M. & Buchner, E. 2013. Strahlenkegel in Opalinuston-Konkretionen des Steinheimer Beckens (Baden-Württemberg). *Zeitschrift der Deutschen Gesellschaft für Geowissenschaften (German Journal of Geosciences)* **164**, 503–13.

Schmieder, M., Trieloff, M., Schwarz, W. H., Buchner, E. & Jourdan, F. 2014. Supportive comment on "Morphology and population of binary asteroid impact craters", by K. Miljković, G. S. Collins, S. Mannick & P. A. Bland, *Earth and Planetary Science Letters* 363 (2013) 121–132 – an updated assessment. *Earth and Planetary Science Letters* **405**, 281–4.

Schultz, P. H. 1994. Chicxulub as an oblique impact. In *Proceedings of the 25th Lunar and Planetary Science Conference*, Houston, TX, 14–18 March 1994, 1211.

Schultz, P. H. & Anderson, R. R. 1996. Asymmetry of the Manson impact structure: Evidence for impact angle and direction. In: The Manson impact structure, Iowa: Anatomy of an impact crater. *Geological Society of America, Special Paper* **302**, 397–417.

Stöffler, D., Artemieva, N. A. & Pierazzo, E. 2002. Modeling the Ries-Steinheim impact event and the formation of the moldavite strewn field. *Meteoritics and Planetary Science* **37**, 1893–907.

von Engelhardt, W., Bertsch, W., Stöffler, D., Groschopf, P. & Reiff, W. 1967. Anzeichen für den meteoritischen Ursprung des Beckens von Steinheim. *Die Naturwissenschaften* **54**, 198–9 (in German).

https://doi.org/10.1017/S0016756817000711 Published online by Cambridge University Press